

Article

Temperature Sensing via Electromagnetically Induced Transparency Vapor

Teh-Chau Liau ¹, Jian-Qi Shen ^{2,*} and Shun-Feng Su ^{1,*}

¹ Department of Electrical Engineering, College of Electrical Engineering and Computer Science, National Taiwan University of Science and Technology, Taipei 106335, Taiwan; d10207302@mail.ntust.edu.tw

² Centre for Optical and Electromagnetic Research, College of Optical Science and Engineering, East Building No. 5, Zijingang Campus, Zhejiang University, Hangzhou 310058, China

* Correspondence: jqshen@zju.edu.cn (J.-Q.S.); sfsu@mail.ntust.edu.tw (S.-F.S.)

Abstract: The behavior of multilevel atomic ensembles (e.g., alkali-metal atoms) can be influenced significantly by the intensity of a driving field (or controlling/coupling field). The phase coherence between two transition pathways driven by a probe light and a driving field can lead to the effect known as electromagnetically induced transparency (EIT). In EIT, the probe light can pass through a three-level alkali-metal atomic vapor without absorption or reflection when two coherent resonances (transition pathways driven by the driving and probe fields) are present and the linewidths of the transparency windows are sufficiently narrow. The optical characteristics of atomic systems can also be affected by the Doppler broadening of the absorption profile in a spectroscopy. Our analysis indicates that both broadenings (related to the transitions excited by the driving and probe fields) can be expanded, leading to an increase in the transmittance and reflectance broadenings when a coupling field with adaptive strength is applied; the corresponding temperature would, thus, be implemented and readable. We show that the most suitable preparation for temperature sensing via an EIT vapor is to provide 80 times the spontaneous decay rate (SDR) of the excited atomic levels. This configuration results in reflectance and transmittance values that range between zero and one and cover a temperature range of 0 K to 600 K. As an example, we demonstrate the integration of specialized coating technologies with EIT ensembles for temperature sensing in the range of dozens of kelvins at and above room temperature. A key advantage of this temperature-sensing system is its ability to use adaptive resonant visible light as the probe field. This novel approach may find applications in providing unprecedented levels of precision and control in temperature sensing for coating processes and in the design of other photonic or optical devices. It can also be used to determine the temperature-dependent behavior of the specific heat of alkali-metal solids and gases (including the latent heats of vaporization or sublimation of alkali-metal solids) through the reflection and transmission spectra of the vaporized EIT atomic vapors.

Keywords: electromagnetically induced transparency (EIT); temperature sensing; spontaneous decay rate (SDR); three-level atomic systems; atomic vapor cell; Doppler broadening



Citation: Liau, T.-C.; Shen, J.-Q.; Su, S.-F. Temperature Sensing via Electromagnetically Induced Transparency Vapor. *Coatings* **2023**, *13*, 1887. <https://doi.org/10.3390/coatings13111887>

Academic Editor: Anna Palau

Received: 21 September 2023

Revised: 24 October 2023

Accepted: 30 October 2023

Published: 2 November 2023



Copyright: © 2023 by the authors. Licensee MDPI, Basel, Switzerland. This article is an open access article distributed under the terms and conditions of the Creative Commons Attribution (CC BY) license (<https://creativecommons.org/licenses/by/4.0/>).

1. Introduction

Temperature sensors are devices that are used to measure the temperature of a gas, material, or environment based on different physical principles. Some notable developments and applications of temperature sensors have recently been achieved [1–6]. For example, in textile-integrated thermocouples [1], two conductors with different Seebeck coefficients can be used to generate a voltage signal proportional to the temperature difference between a hot and a cold junction. The conductors are embedded in various textile substrates, such as cotton, cellulose, polymers, carbon, or optical fibers, to form flexible and wearable temperature sensors. In nanocomposite-based capacitive gas sensors [2], nanocomposite materials composed of pyrrole-bromo aluminum phthalocyanine can be

used as a sensing layer, and interdigitated electrodes are used as the capacitive elements. The capacitance of the sensor changes when exposed to different gases or vapors due to the variation in the dielectric constant of the sensing layer. These sensors can detect H₂S gas at room temperature (approximately 25 °C) with a fast response and good stability. In fabric nanocomposite resistance temperature detectors (RTDs) [3], a nanocomposite material made of electrospun nylon-6 functionalized with multiwalled carbon nanotubes (MWCNTs) and polypyrrole (PPy) can be used as a sensing layer, with silver electrodes as the resistive elements. The resistance of the sensor increases linearly with temperature, acting like an RTD. In all-printed composite thermistors [4], a composite material consisting of carbon black and polyvinylidene fluoride (PVDF) acts as the sensing layer and silver electrodes serve as the resistive elements, where the resistance of the sensor decreases exponentially with temperature, acting like a thermistor. In distantly scanning infrared sensors [5], thin films of materials such as silicon nitride (SiN), deposited via plasma-enhanced chemical vapor deposition (PECVD) onto a substrate, are used as the sensing elements. This sensor possesses the ability to swiftly scan and identify the infrared radiation discharged by each object at adaptive distances, contingent upon their individual temperatures, and can transmute the information into corresponding electrical signals in sequence. It can be used to measure the temperature of a human body through the infrared radiation emitted by the skin. In the distributed in-tube condensation of low-global-warming-potential (GWP) refrigerant fiber-optic sensors [6], fiber-optic cables act as sensing elements and measure the backscattered light signals along the length of the cables. These sensors can be used to measure the temperature profile along a tube during the condensation of a low-GWP refrigerant. Fiber-optic sensors can typically measure temperatures over a wide range, from cryogenic temperatures to several hundred degrees Celsius.

In this paper, we suggest a different temperature-sensing scheme using an electromagnetically induced transparency atomic vapor (e.g., a three-level alkali-metal atomic gaseous medium). In the literature on quantum optics [7–12], the effect of phase coherence in atomic-level transitions shows that some novel phenomena, such as electromagnetically induced transparency (EIT) and atomic coherent population trapping (CPT), can be used to flexibly control electromagnetic wave propagation through multilevel atomic media [7–12]. The width of EIT resonance has been studied in alkali-metal atomic media such as rubidium vapor [13], and experiments have been performed to slow down and shape single-photon light pulses and generate pulses suitable for quantum key distribution applications [14], which can be used to test some approaches for single-photon storage. The phenomena of Doppler broadening in the optical transitions of atomic vapors, encompassing both ballistic and diffusive atomic movements within a confined interaction region, as well as collision-induced depopulation and decoherence, have been comprehensively elucidated [15]. Resonance transmission in a three-level Lambda-type system of rubidium's D1 line can be controlled by adjusting the linewidth of the pumping (coupling) laser field [16]. The steady-state EIT and sub-Doppler linewidth in Doppler-broadened Lambda-type ⁸⁷Rb formed on the D2 line transition have been experimentally determined [17]. A narrow dip in the absorption spectrum undergoes substantial narrowing compared with an atom at rest when particle motion influences two-photon resonances and ensures further extension beyond the residual Doppler shift [18]. The intensity of the generated coherent radiation from a laser without inversion for the Vee and Lambda configurations in a Doppler-broadened medium has been numerically calculated for a wide range of experimental parameters [19–22]. The dependence of the transmission linewidth on the driving-field intensity has been characterized and regarded as a “degree of optical pumping” [23]. It has been demonstrated that the reflection and transmission of electromagnetic pulses through dielectrics doped with three-level atomic systems [24,25] or quantum-dot-molecule films [26] can be varied by changing the thickness of the slab or the intensity of the coupling field. Some information on the three energy levels of typical neutral atoms [27–30] for producing the EIT effect can be found in Appendix A. The theoretical foundation of the principles used in the temperature sensing

in this work includes the quantum optical method [7] for the atomic-level density matrix, thermodynamics and statistical principles [31], and optical media electromagnetics [32].

According to the Standard Guide for Painting Inspectors (Metal Substrates), ASTM Designation D 3276-86 [33], for the coating process, it is very important to control and measure the temperature to achieve the desired outcome. The maximum surface temperature for coating applications is typically 125 °F (50 °C) unless specified otherwise. If the surface is very hot, the coating solvents may evaporate quickly, hindering application and potentially resulting in blistering or porous films. Conversely, lower ambient temperatures can lead some paints to thicken, which can increase the drying time and result in running or sagging. The lowest temperature typically used is 50 °F (10 °C). These temperature parameters are crucial for ensuring the effectiveness and durability of the coating.

2. Materials and Methods

In our scenario, a small amount of alkali-metal solid is present in a glass cell (also referred to as an “atomic vapor cell”). When the temperature increases, the solid in the cell sublimates to a gaseous state; i.e., a three-level EIT atomic vapor is enclosed in the glass cell. The saturated vapor concentration of the alkali-metal atoms in the glass cell is a function of temperature. Because the optical properties of the alkali-metal atomic vapor are determined by the saturated vapor concentration and the external control-field intensity, reflection and transmission (for the incident probe light) by the atomic vapor in the glass cell can be manipulated by changing the temperature and the adjustable external control field.

In the absence of a driving laser beam, the vapor behaves like a typical gas [7]. The velocity of the atomic ensembles follows a normal distribution, and the absorbance linewidth is rendered. When a driving laser beam is applied, the atoms move faster, their kinetic energy increases, and the temperature of the vapor rises. This results in a transparency dip at the center of the absorbance profile. Various types of broadening become pronounced. By measuring any type of broadening in the spectral lines and inspecting the reflectance and the transmittance of the probe field crossing the EIT vapor slab, the temperature function of the atomic vapor can be determined.

2.1. The Relative Dielectric Constant of a Typical EIT Vapor

Here, we first consider the optical or electromagnetic response of an EIT atomic vapor [7]. Let us consider a three-level Lambda-type atomic or ensemble system, with two lower levels, $|1\rangle$, $|2\rangle$, and one upper level, $|3\rangle$ (see Figure 1a for a schematic diagram). This atomic ensemble system is driven by a probe light and a control field, which excite the $|1\rangle - |3\rangle$ and $|2\rangle - |3\rangle$ transitions, respectively. Because the atomic levels $|1\rangle$ and $|2\rangle$ have the same parity, and the upper level, $|3\rangle$, has an opposite parity to levels $|1\rangle$ and $|2\rangle$, an electric-dipole-allowed transition can occur between levels $|1\rangle$ and $|3\rangle$ and can also occur between levels $|2\rangle$ and $|3\rangle$, but it cannot occur between levels $|1\rangle$ and $|2\rangle$, because the two levels $|1\rangle$ and $|2\rangle$ (having the same parity) belong to the states that have the same principal quantum number, and their energy levels (energy eigenvalues) are almost degenerate. In general, such a three-level system can be demonstrated or found in alkali-metal atoms (e.g., Li, Na, K, and Rb). By using the quantum-mechanical density matrix approach, the complex microscopic electric susceptibility (caused by the $|1\rangle - |3\rangle$ transition driven by the probe field) of an alkali-metal atomic vapor is given by [7]

$$\chi = N_a \beta = N_a \left(i \frac{|\wp_{13}|^2}{\epsilon_0 \hbar} \frac{[\frac{\gamma_2}{2} + i(\Delta_p - \Delta_c)]}{\left(\frac{\Gamma_3}{2} + i\Delta_p\right) [\frac{\gamma_2}{2} + i(\Delta_p - \Delta_c)] + \frac{|\Omega_c|^2}{4}} \right) \quad (1)$$

where N_a denotes the atomic concentration (number density per unit volume), \wp_{13} is the electrical dipole moment between states $|1\rangle$ and $|3\rangle$, Γ_3 is the spontaneous decay rate (SDR), γ_2 is the collisional dephasing rate (CDR), Ω_c is the Rabi frequency of the control field, \hbar is the Planck constant, and ϵ_0 is the absolute dielectric constant of a vacuum. Here, Ω_c is

defined as $\Omega_c = \wp_{32} E_c / \hbar$, where E_c is the control-field envelope (slowly varying amplitude of its electric field). The two frequency detunings (related to the transitions $|1\rangle - |3\rangle$ and $|2\rangle - |3\rangle$) are defined as $\Delta_p = \omega_{31} - \omega_p$ and $\Delta_c = \omega_{32} - \omega_c$, with ω_p and ω_c being the angular frequencies of the probe field and the control field, respectively.

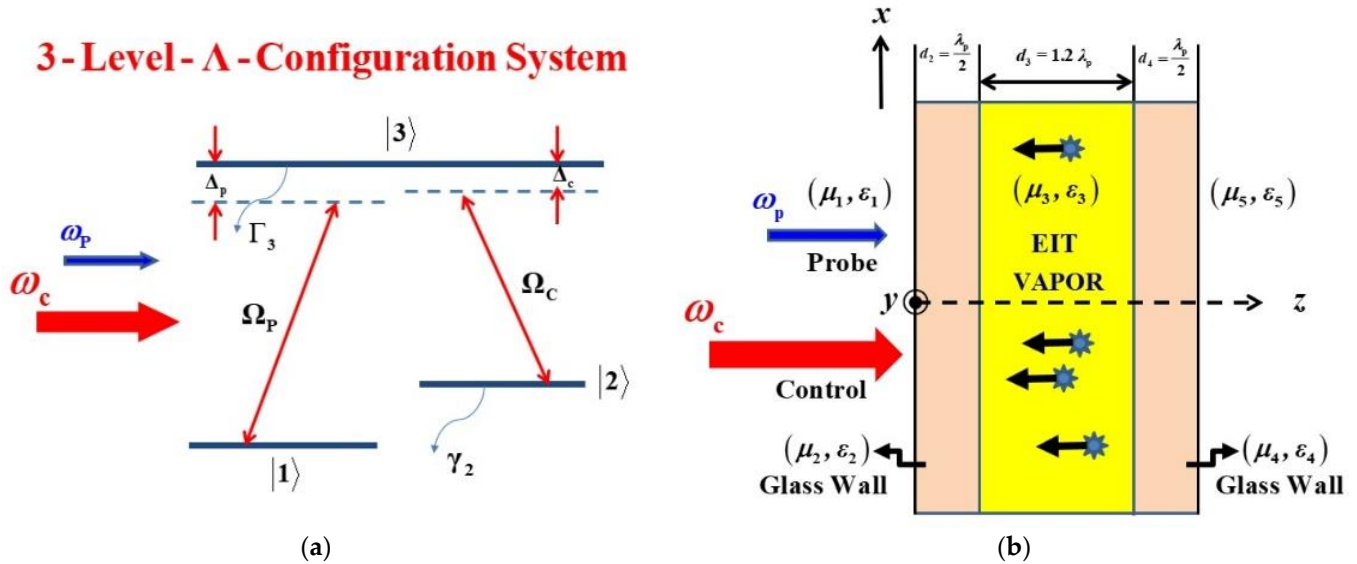


Figure 1. The fundamental mechanism of temperature sensing using a three-level atomic system. (a) Schematic diagram of a three-level Lambda-type atomic system; (b) 1.2-wavelength-thick EIT atomic vapor slab sandwiched by two glass walls, with dielectric constant $\epsilon_2 = \epsilon_4 = 4$ and thickness $d_2 = d_4 = \lambda_p/2$ (all three layers embedded in vacuum). The alkali-metal solid is placed into a glass cell or plated on the inner walls of a glass cell. When the temperature increases, the alkali-metal solid sublimates into atomic vapor, increasing the three-level atomic number density of the vapor. This modifies the optical characteristics of the three-level atomic vapor in response to the probe light that drives the $|1\rangle - |3\rangle$ transition.

Now, let us consider the Doppler effect. The frequency shifts for the three transition frequencies can be expressed as follows:

$$\omega_{31}^D = \omega_{31} \left(1 \pm \frac{v}{c}\right), \quad \omega_{21}^D = \omega_{21} \left(1 \pm \frac{v}{c}\right), \quad \omega_{32}^D = \omega_{32} \left(1 \pm \frac{v}{c}\right). \quad (2)$$

In this expression, + and – denote that the probe and control lights are propagating toward and away from the moving atomic ensembles, respectively. In this study, we assume that their traveling directions are all in counter-propagation. Three new Doppler-dependent detuning quantities can then be obtained as follows:

$$\Delta'_p = \Delta_p + \left(\frac{\omega_{31}}{c}\right)v, \quad \Delta'_c = \Delta_c + \left(\frac{\omega_{32}}{c}\right)v, \quad \Delta'_p - \Delta'_c = (\Delta_p - \Delta_c) + \left(\frac{\omega_{21}}{c}\right)v. \quad (3)$$

Let the spontaneous decay rate of level $|3\rangle$ $\Gamma_3 = 2 \times 10^7 \text{ s}^{-1}$, the dephasing rate $\gamma_2 = \frac{\Gamma_3}{200}$, and the electric dipole moment $|\wp_{13}| = 10^{-29} \text{ C} \cdot \text{m}$. Some dimensionless quantities (related to frequency detuning and Rabi frequency) are defined as $x = \frac{\Delta_p}{\Gamma_3}$, $y = \frac{\Delta_c}{\Gamma_3}$, and $z = \frac{|\Omega_c|}{\Gamma_3}$. We substitute Equation (3) into Equation (1), and the Doppler-modified susceptibility (caused by the $|1\rangle - |3\rangle$ transition driven by the probe field [7]) can be expressed as

$$\chi = N_a \beta = N_a \left(i \frac{|\wp_{13}|^2}{\epsilon_0 \hbar} \frac{\left[\frac{\Gamma_3}{400} + i(\Delta'_p - \Delta'_c) \right]}{\left(\frac{\Gamma_3}{2} + i\Delta'_p \right) \left[\frac{\Gamma_3}{400} + i(\Delta'_p - \Delta'_c) \right] + \frac{1}{4} |\Omega_c|^2} \right) \quad (4)$$

This can be rewritten as

$$\chi = N_a \beta = N_a \left(\frac{|\rho_{13}|^2}{\epsilon_0 \hbar \Gamma_3} \frac{\left[i \frac{1}{400} - \left(\frac{\Delta'_p - \Delta'_c}{\Gamma_3} \right) \right]}{\left(\frac{1}{2} + i \frac{\Delta'_p}{\Gamma_3} \right) \left[\frac{1}{400} + i \left(\frac{\Delta'_p - \Delta'_c}{\Gamma_3} \right) \right] + \frac{1}{4} \frac{|\Omega_c|^2}{\Gamma_3^2}} \right). \tag{5}$$

Thus, the Doppler-modified susceptibility is given by

$$\chi = N_a \frac{|\rho_{13}|^2}{\epsilon_0 \hbar \Gamma_3} \left(\frac{\left[i \frac{1}{400} - \left(\frac{\Delta_p - \Delta_c}{\Gamma_3} + \frac{\omega_{21} v}{\Gamma_3} \right) \right]}{\left(\frac{1}{2} + i \left(\frac{\Delta_p + \frac{\omega_{31} v}{\Gamma_3}}{\Gamma_3} \right) \right) \left[\frac{1}{400} + i \left(\frac{\Delta_p - \Delta_c}{\Gamma_3} + \frac{\omega_{21} v}{\Gamma_3} \right) \right] + \frac{1}{4} \frac{|\Omega_c|^2}{\Gamma_3^2}} \right). \tag{6}$$

The new complex bulk susceptibility of the three-level atomic vapor [7] can thus be rewritten as

$$\chi_{\text{new}} = [K_0 N'_a(T)] \left(\frac{\left\{ -[(x - y) + k_{21}v] + i \frac{1}{400} \right\}}{\left\{ \frac{1}{2} + i[x + k_{31}v] \right\} \left\{ \frac{1}{400} + i[(x - y) + k_{21}v] \right\} + \frac{1}{4} z^2} \right), \tag{7}$$

where the parameters are given by $K_0 = \frac{|\rho_{13}|^2}{\epsilon_0 \hbar \Gamma_3}$, $N'_a(T) = N_0 \frac{T_0}{T} \exp \left[-\frac{l}{k_B} \left(\frac{1}{T} - \frac{1}{T_0} \right) \right]$ (in $\frac{\text{Atom}}{\text{m}^3}$) [31], $T_0 = 300 \text{ K}$, $N_0 = 1 \times 10^{22} \text{ m}^{-3}$, $l = 10^{-21} \text{ J}$, $k_B = 1.38 \times 10^{-23} \text{ J/K}$, $k_{31} = \frac{\omega_{31}}{c \Gamma_3}$, $k_{32} = \frac{\omega_{32}}{c \Gamma_3}$, $k_{21} = \frac{\omega_{21}}{c \Gamma_3}$.

There are some examples of three-level Lambda configurations of EIT atomic ensembles with different Doppler-shift parameters k_{31} , k_{21} , and k_{32} . Readers can refer to Appendix A.

In this paper, we assume that the atomic ensemble has a mass of 10 amu (atomic mass unit); k_{31} , k_{32} , and k_{21} are 1.1 s/m, 1.1 s/m, and $1.1 \times 10^{-6} \text{ s/m}$, respectively; $x = 1$, $y = 0$, $z = [0, 10, 50, 60, 70, 80, 90, 100]$ (eight cases); $T = [1 \text{ K} - 600 \text{ K}]$, and thus, $K_0 = 5.3578 \times 10^{-21} \left(\frac{\text{m}^3}{\text{Atom}} \right)$.

The expression for the susceptibility $Ex[\chi] = \sqrt{\frac{m}{2\pi k_B T}} \int_{-\infty}^{+\infty} \chi_{\text{new}} \exp \left[-\frac{mv^2}{2k_B T} \right] dv$ for EIT ensembles has been numerically integrated using the trapezoidal rule in the scope of temperature (see Figure 2a).

Applying the Clausius–Mossotti relation [32], we obtain the final dimensionless complex relative dielectric constant as follows:

$$\epsilon_3 = \epsilon_3(T) = 1 + \frac{N'_a(T) \beta'(T)}{1 - \frac{N'_a(T) \beta'(T)}{3}} = 1 + \chi'(T) + i\chi''(T). \tag{8}$$

2.2. FWHM of Transparency Windows

The full width at half maximum (FWHM) of Doppler broadening in the atomic velocity domain for a typical gas absorption profile is equal to a specific value ($2\sqrt{(k_B T \ln 2)/m}$). This value can be broadened by an increase in the square root of the temperature and a decrease in the square root of the mass of each atom. However, for an EIT vapor, when a monochromatic weak probe laser beam is tuned to a two-level atomic transition resonance, the levels $|1\rangle, |3\rangle$ under consideration would be strongly mixed with another coupling or driving laser field (the Rabi frequency Ω_c plays the role of the superposition coefficient in this coupling). This leads to splitting due to the AC Stark effect and results in an Autler–Townes doublet for a three-level Lambda-type system [7]. A much smaller transparency linewidth with a deep dip is rendered, which is almost Doppler-free when the driving laser beam and the probe laser beam have nearly the same wavelength and propagate collinearly through the vapor [17–20]. The coherent resonance results in only a

very small anti-absorbed variation (transparency linewidth) appearing in the middle of the absorption profile.

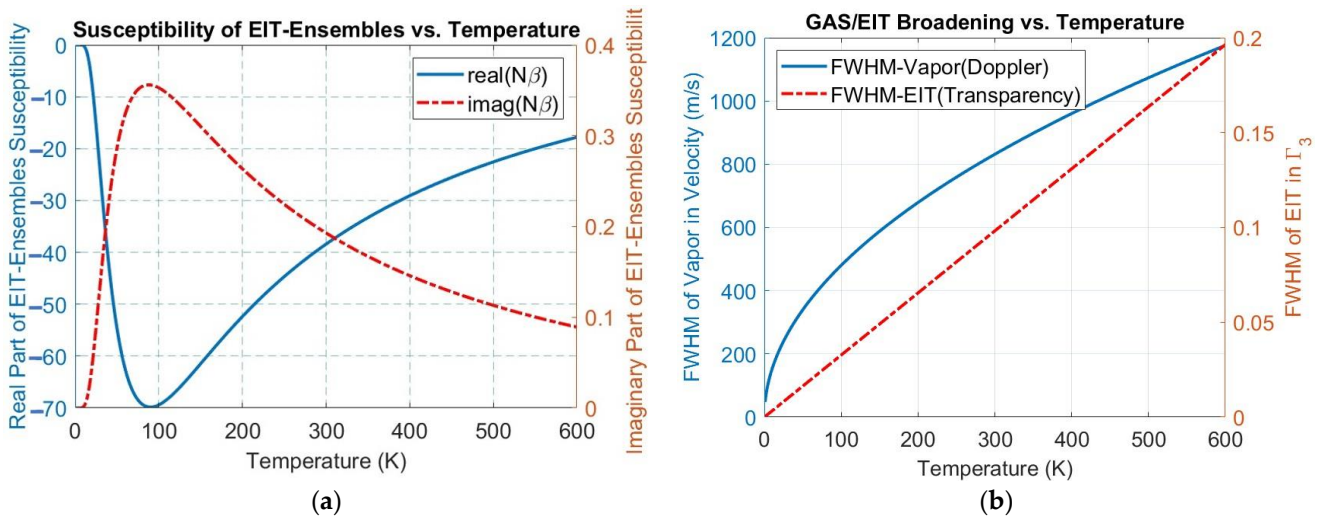


Figure 2. Theoretical curves for temperature sensing. (a) Variation in three-level atomic vapor susceptibility of EIT ensemble versus kelvin temperature (K) under various conditions; (b) comparison between the full width at half maximum (FWHM) with Doppler broadening (in atomic velocity domain) and EIT transparency windows’ FWHM without Doppler broadening (in Γ_3) versus kelvin temperature (K).

The expected linear susceptibility has been acquired as a single-peak Lorentzian profile by timing Maxwell’s velocity distribution profile and shown as an analytical error function in some studies [15–17]. Instead of using this expression, we calculate the expected value via trapezoidal numerical integration. The Doppler-free FWHM of the transparency window can be found by using some simple algebra. As mentioned in the last section, the imaginary part $\text{Im}[\chi]$ of the three-level atomic vapor susceptibility (caused by the $|1\rangle - |3\rangle$ transition driven by the probe light) can be extracted through the factor F of the susceptibility

$$F = \frac{\left[\frac{\gamma_2}{2} + i(\Delta_p - \Delta_c)\right]}{\left(\frac{\Gamma_3}{2} + i\Delta_p\right)\left[\frac{\gamma_2}{2} + i(\Delta_p - \Delta_c)\right] + \frac{|\Omega_c|^2}{4}}. \tag{9}$$

When the frequency detuning $\Delta_p = \Delta_c = 0$ and the control-field Rabi frequency square $|\Omega_c|^2$ is much less than $\frac{\gamma_2}{2} \cdot \frac{\Gamma_3}{2}$ or $|\Omega_c| = 0$, we can have the imaginary part

$$\text{Im}[\chi] \propto \frac{\left[\frac{\gamma_2}{2}\right]}{\left(\frac{\Gamma_3}{2}\right)\left[\frac{\gamma_2}{2}\right] + \frac{|\Omega_c|^2}{4}} = \frac{2}{\Gamma_3} \approx \max(A), \tag{10}$$

where A is the absorption of the slab. When the frequency detuning $\Delta_p = \Delta_c = 0$ and $\frac{|\Omega_c|^2}{4}$ is much larger than $\left(\frac{\Gamma_3}{2}\right)\left(\frac{\gamma_2}{2}\right)$, the imaginary part of the susceptibility is

$$\text{Im}[\chi] \propto \frac{2\gamma_2}{|\Omega_c|^2} \approx 0. \tag{11}$$

Now, let us formulate the real FWHM of the absorption dip profile. For the sake of simplicity, we assume $x = \frac{\Delta_p}{\Gamma_3} \neq 0$, $y = \frac{\Delta_c}{\Gamma_3} = 0$, keep Ω_c as a normal notation, and

choose the dephasing rate γ_2 as a negligibly small constant ($\gamma_2 = \frac{\Gamma_3}{200} \rightarrow 0$). Then, the susceptibility can be expressed as a proportional form of the following expression:

$$iF \rightarrow i\frac{1}{\Gamma_3} \cdot \frac{i\frac{\Delta_P}{\Gamma_3}}{\left(\frac{1}{2} + i\frac{\Delta_P}{\Gamma_3}\right)\left(i\frac{\Delta_P}{\Gamma_3}\right) + \frac{|\Omega_c|^2}{4\Gamma_3^2}} = \frac{1}{\Gamma_3} \cdot \frac{-x}{\left(\frac{1}{2} + ix\right)(ix) + \frac{z^2}{4}} \tag{12}$$

$$= \frac{1}{\Gamma_3} \cdot \frac{-x}{\frac{z^2}{4} - x^2 + \frac{i}{2}x} = \frac{1}{\Gamma_3} \cdot \frac{-x\left(\frac{z^2}{4} - x^2 - \frac{i}{2}x\right)}{\left(\frac{z^2}{4} - x^2\right)^2 + \frac{x^2}{4}}$$

Thus, the main structure of the three-level atomic vapor susceptibility (caused by the |1⟩ – |3⟩ transition driven by the probe light) can be written as

$$\chi = \text{Re}[\chi] + i \times \text{Im}[\chi] \propto \frac{1}{\Gamma_3} \cdot \frac{\left(x^3 - x\frac{z^2}{4}\right) + i\frac{x^2}{2}}{\left(\frac{z^2}{4} - x^2\right)^2 + \frac{x^2}{4}} \tag{13}$$

To find the FWHM point, we require the imaginary part of the susceptibility to be equal to $\frac{1}{\Gamma_3}$ (i.e., $\left(\frac{2}{\Gamma_3} - 0\right)/2 = \frac{1}{\Gamma_3}$), i.e.,

$$\text{Im}[\chi] \propto \frac{1}{\Gamma_3} \cdot \frac{\frac{x^2}{2}}{\left(\frac{z^2}{4} - x^2\right)^2 + \frac{x^2}{4}} = \frac{1}{\Gamma_3} \tag{14}$$

Then, we can obtain the equation

$$\left(\frac{z^2}{4} - x^2\right)^2 + \frac{x^2}{4} = \frac{x^2}{2} \tag{15}$$

Rearranging the equation, we obtain a quadratic equation of x , i.e.,

$$x^4 - \left(\frac{z^2}{2} + \frac{1}{4}\right)x^2 + \frac{z^4}{16} = 0 \Rightarrow x^2 = \frac{\frac{z^2}{2} + \frac{1}{4} \pm \sqrt{\frac{1}{16} + \frac{z^2}{4}}}{2} \tag{16}$$

Solving the quadratic equation of x , we obtain the roots

$$x = \pm \sqrt{\frac{2z^2 + 1 \pm \sqrt{4z^2 + 1}}{8}} \tag{17}$$

There are four roots:

$$x_{4,1} = \pm \sqrt{\frac{2z^2 + 1 + \sqrt{4z^2 + 1}}{8}}, x_{3,2} = \pm \sqrt{\frac{2z^2 + 1 - \sqrt{4z^2 + 1}}{8}} \tag{18}$$

We ignore the left-most root, x_1 , and the right-most root, x_4 , of Equation (18), and then the static FWHM of the transparency windows (without the Doppler effect) can be adopted with the value of the difference between the third and second roots of Equation (18), i.e.,

$$\Delta x = x_3 - x_2 = \sqrt{\frac{2z^2 + 1 - \sqrt{4z^2 + 1}}{2}} \tag{19}$$

This means that the FWHM of the EIT transparency window in Γ_3 is a function of either $z = |\Omega_c|/\Gamma_3$ or of the temperature according to $T = (\hbar|\Omega_c|)/k_B = (\hbar\Gamma_3/k_B)z$. We combine the FWHM curve of the atomic root-mean-square velocity with Doppler broadening and the FWHM curve of the EIT transparency window without Doppler broadening, both of

which increase with temperature. The relevant comparison of the two curves is shown in Figure 2b.

When a stronger driving field (with the Rabi frequency Ω_c) that drives the $|2\rangle - |3\rangle$ transition is applied, the velocity of the moving atoms may be greater (with an increase in the root-mean-square speed according to $v_{rms} = \sqrt{(2k_B T)/m}$), and they may have an elevated temperature (i.e., $T \propto (\hbar|\Omega_c|)/k_B$). In other words, when the direction of the driving light (Ω_c) propagates toward the moving atoms (i.e., approaching them), the Doppler effect can broaden the FWHM of the transparency window of the probe light (see Figure 3a–h).

2.3. Reflectance, Transmittance, and Absorption

We will discuss the problem of light reflection, transmission, and absorption in a system consisting of a vapor slab with thickness d_3 and an intense control field applied, as schematically shown in Figure 1b. The transfer matrix of the j -th layer can be expressed as [21,22]

$$Q_j(\omega_p, d_j) = \begin{bmatrix} \cos(k_z^j d_j) & i \cdot \sin(k_z^j d_j)/r_j \\ i \cdot r_j \sin(k_z^j d_j) & \cos(k_z^j d_j) \end{bmatrix}, \quad (j = 2, 3, 4) \tag{20}$$

where $k_z^j = \sqrt{k_p^2 \epsilon_j}$ is the z component of the wave number in the j -th layer; $r_j = k_z^j/k_p$; d_j is the thickness of the j -th layer; k_p is the wave number of the probe field ($k_p = \omega_p/c$); and c is the speed of light in a vacuum. The total transfer matrix for the considered glass cavity system is given by

$$P(\omega_p) = Q_2(\omega_p, \epsilon_2, d_2)Q_3(\omega_p, \epsilon_3, d_3)Q_4(\omega_p, \epsilon_4, d_4). \tag{21}$$

In our scheme for temperature sensing with a three-level atomic vapor, the alkali-metal solid is placed into a glass cell (or plated on the inner wall of the glass cell). As the temperature rises, the alkali-metal solid sublimates into atomic vapor, thus increasing the atomic number density of the gas in the cell. This modifies the dielectric coefficient and susceptibility and, thus, changes the optical properties of the atomic vapor (in response to the probe light that drives the $|1\rangle - |3\rangle$ transition). We assume that the glass walls on both sides of the atomic vapor cell have a relative dielectric constant ϵ_r equal to 4 and a thickness equal to half of the probe light wavelength ($\lambda_p/2$), such that $Q_2(\omega_p, \epsilon_2, d_2) = Q_4(\omega_p, \epsilon_4, d_4) = \begin{bmatrix} 1 & 0 \\ 0 & 1 \end{bmatrix}$, which is an all-transmission characteristic. The probe light travels in the z -direction from medium 1 (left-side half-space), impinges normally on the first left vertical side boundary of the glass cell, passes through the slab (atomic vapor cell), crosses the last right vertical side boundary of the glass cell, and finally transmits into medium 5 (right-side half-space). We assume that media 1 and 5 are in a vacuum, media 2 and 4 have a relative permittivity of $\epsilon_2 = \epsilon_4 = 4$, medium 3 has $\epsilon_3 = \epsilon_{EIT}$, and all five regions are nonmagnetic (i.e., $\mu_j = 1, j = 1, 2, 3, 4, 5$). The reflection coefficient at the left-side interface of the vapor slab is given by [15–17]

$$r(k_p) = \frac{r_1(P_{22} - P_{11}) - (r_1^2 P_{12} - P_{21})}{r_1(P_{22} + P_{11}) - (r_1^2 P_{12} + P_{21})} = \frac{-\frac{1}{2} \left(\frac{1}{\sqrt{\epsilon_3}} - \sqrt{\epsilon_3} \right) \sin(k_p \sqrt{\epsilon_3} d_3)}{\cos(k_p \sqrt{\epsilon_3} d_3) - \frac{1}{2} \left(\frac{1}{\sqrt{\epsilon_3}} + \sqrt{\epsilon_3} \right) \sin(k_p \sqrt{\epsilon_3} d_3)}, \tag{22}$$

and the transmission coefficient at the right side of the vapor slab is

$$t(k_p) = \frac{2r_1}{r_1(P_{22} + P_{11}) - (r_1^2 P_{12} + P_{21})} = \frac{1}{\cos(k_p \sqrt{\epsilon_3} d_3) - \frac{1}{2} \left(\frac{1}{\sqrt{\epsilon_3}} + \sqrt{\epsilon_3} \right) \sin(k_p \sqrt{\epsilon_3} d_3)}. \tag{23}$$

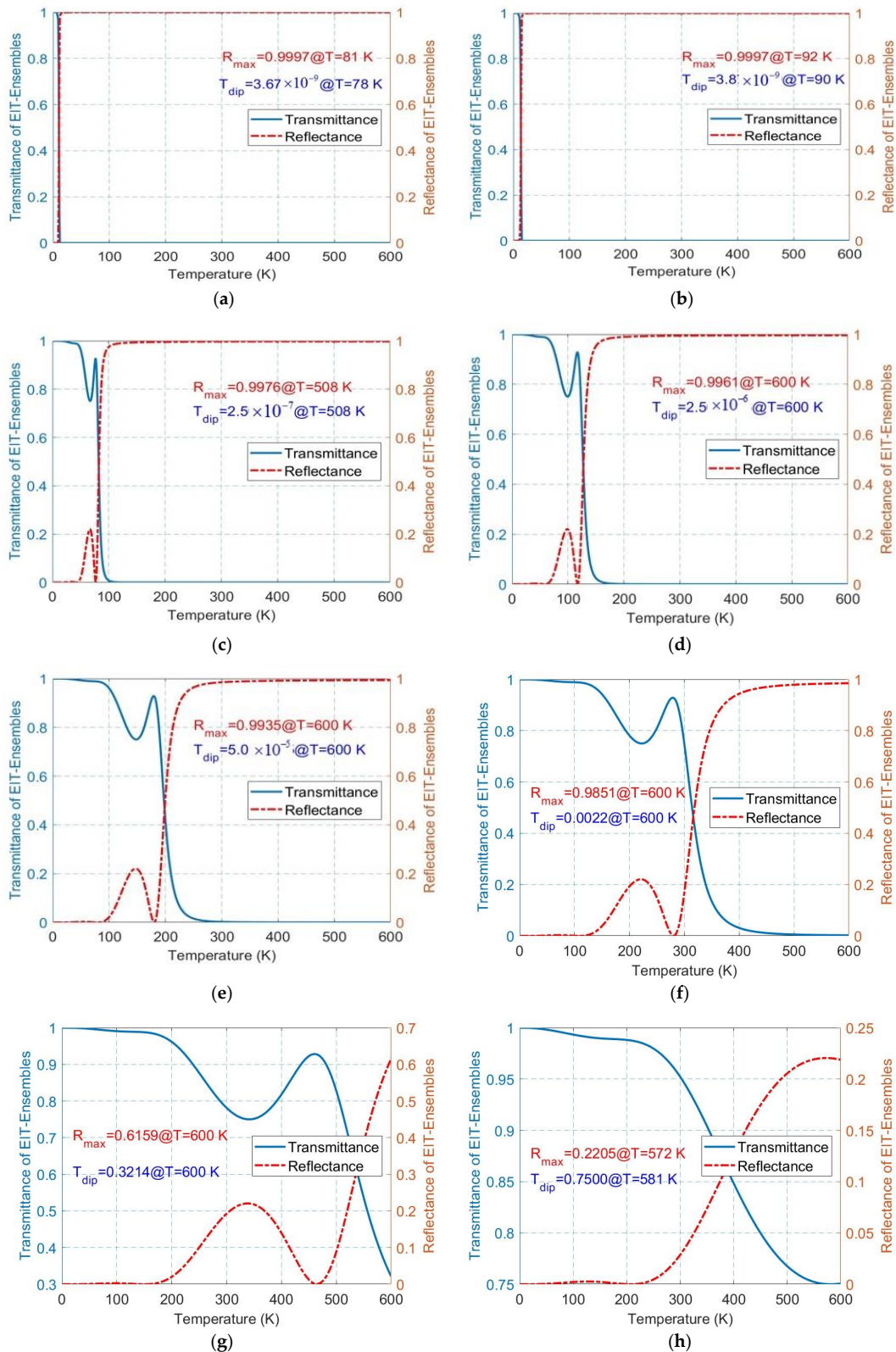


Figure 3. The variation in reflectance and transmittance broadening in temperature-sensing scope under the same prerequisite conditions $x = \Delta_p/\Gamma_3 = 1$, and $y = \Delta_c/\Gamma_3 = 0$ but several different $z = |\Omega_c|/\Gamma_3$: (a) $z = 0$, (b) $z = 10$, (c) $z = 50$, (d) $z = 60$, (e) $z = 70$, (f) $z = 80$, (g) $z = 90$, and (h) $z = 100$. The blue line in (a–h) represents the normal variation in transmittance due to temperature changes, while the red dashed line denotes the variation in reflectance due to temperature changes. One of the insets in each figure is a legend that describes the meaning of the two lines. The other inset describes the largest value of reflectance R_{max} and the minimum value of transmittance T_{dip} for each corresponding temperature in detail and accuracy.

Therefore, the reflectance on the left side, transmittance on the right side, and absorption in the region of the three-level atomic vapor slab (glass cell) can then be expressed, respectively, as

$$R = |r(k_p)|^2, \quad T_{\text{tran}} = |t(k_p)|^2, \quad \text{and} \quad A = 1 - R - T_{\text{tran}}. \quad (24)$$

3. Results

For a neutral atomic ensemble vapor slab, the broadening of the transparency window increases with the intensity of the driving field (with the Rabi frequency Ω_c) that drives the $|2\rangle - |3\rangle$ transition. This process also results in an elevation in temperature. As the intensity of the driving field increases, the transparency window versus temperature accordingly widens (see Figure 2b). This means that the distance between the Autler–Townes doublet in the double optical resonance can be observed as temperature broadening (and thus the FWHM of the absorption). The variations in the reflectance broadening and transmittance broadening have been calculated for several tens of times the magnitude of Ω_c of the strong driving fields as a function of temperature and are shown in Figure 3a–h. For temperature-sensing applications, proper preparation involves driving-field strengths of 50, 60, 70, and 80 times the spontaneous decay rate (SDR), i.e., $z = |\Omega_c|/\Gamma_3 = 50\text{--}80$. At these driving-field strengths (Ω_c), the system exhibits both reflectance and transmittance values ranging from 0 to 1, corresponding to temperatures of 100 K, 200 K, 300 K, and 600 K, respectively. The entire temperature sensor can be equipped with a sensitive photodiode to detect small variations in the weak probe light. These micro-level signals can then be amplified with an electronic differential amplifier and clearly displayed. This allows for more precise measurements and a better understanding of the effect of the driving field on the transparency window. By carefully manipulating parameters such as the thickness of the EIT vapor slab or glass wall, the concentration of the ensembles, and the sensitivity of the electronic devices, temperature-sensing systems may be optimized for various applications. For instance, altering the thickness of the EIT vapor slab or glass wall, adjusting the concentration of ensembles, increasing the sensitivity of electronic devices, or specifying other combinations of these conditions could yield different temperature-sensing data that could be useful in photonic device design and industrial applications. In principle, susceptibility is a critical material parameter that governs the behavior of an EIT material. Understanding this parameter can help clarify the underlying physical mechanisms and pave the way for new sectionalized temperature detection of the EIT vapor slab. The transmittance and reflectance of the probe light (driving the atomic $|1\rangle - |3\rangle$ transition) over a vapor slab are influenced by both Doppler broadening and transparency windows broadening, which have been numerically calculated by using simple algebraic methods. Under the same prerequisite conditions of $x = \Delta_p/\Gamma_3 = 1$ and $y = \Delta_c/\Gamma_3 = 0$ with different driving fields $z = \Omega_c/\Gamma_3 = 0, 10$ (exciting the $|2\rangle - |3\rangle$ transition), the transmittance can drop abruptly from 1 to 0, while the reflectance abruptly increases from 0 to 1 at temperatures 12 K and 15 K, respectively (clearly, this has simply a toy-model meaning because the theoretical equations for the atomic systems presented in this paper would be invalid at such ultra-low temperature). This configuration results in a very low resolution for discriminating differences in transmittance and reflection data (see Figure 3a,b). If, however, the driving field (exciting the $|2\rangle - |3\rangle$ transition) is adjusted to be $z = \Omega_c/\Gamma_3 = 50, 60, 70$, the transmittance curve can vary abruptly from 1 to 0, and the reflectance curve can vary abruptly from 0 to 1 simultaneously at temperatures of 100 K, 200 K, and 300 K, respectively (see Figure 3c–e). While the driving field is tuned to be $z = \Omega_c/\Gamma_3 = 80$, the excellent resolution (transmittance and reflectance are distributed between zero and one) can be achieved, covering the entire temperature range from $T = 0$ K to 600 K (see Figure 3f). If the applied driving field becomes more intense, e.g., $z = \Omega_c/\Gamma_3 = 90, 100$, the transmittance and reflectance range would become smaller such that the resolution falls to an undistinguishable level (see Figure 3g,h).

However, there are some limitations and challenges that need to be addressed for this method to be widely applicable. First, we need to ensure that the vapor slab is maintained at a stable temperature and pressure to avoid fluctuations in the atomic density and velocity distribution. Second, we need to consider the effects of Doppler broadening, power broadening, collisional broadening, and Zeeman splitting on the spectral features and line shapes. Third, we need to account for nonlinear effects, such as saturation, self-phase modulation, four-wave mixing, and electromagnetically induced absorption, that may occur at high driving-field intensities. Fourth, we need to calibrate the temperature sensor with a standard reference thermometer and evaluate its accuracy, precision, sensitivity, stability, repeatability, and reproducibility. Fifth, we need to compare our method with other existing methods, such as thermocouples, thermistors, pyrometers, bolometers, and optical fibers. Finally, we need to explore other possible applications of this method, such as optical switching, modulation, filtering, amplification, lasing, and quantum information processing.

4. Discussion

The optimal temperature for applying coatings is contingent upon the specific type of coating being used. Generally, coatings should be applied in favorable weather conditions, when the air and surface temperatures are between 50 °F (10 °C) and 125 °F (50 °C) [33], for most paints. In Table 1, it is shown that under the conditions $x = \Delta_p/\Gamma_3 = 1$, $y = \Delta_c/\Gamma_3 = 0$, and $z = \Omega_c/\Gamma_3 = 0, 50$, the reflectance data are very close to 1, and the transmittance data are very small, i.e., approaching 0 (e.g., at an order of magnitude of 10^{-7} and 10^{-9}). Such data do not have practical significance: i.e., they are understood only in the sense of a model. With these very small ranges, discriminating the corresponding temperature is difficult. When the conditions $x = \Delta_p/\Gamma_3 = 1$, $y = \Delta_c/\Gamma_3 = 0$, and $z = |\Omega_c|/\Gamma_3 = 80$ are met, both the reflectance and transmittance can be easily distinguished, with values of 0.565782 and 0.557437, respectively, covering operating temperatures of 283 K to 323 K. In contrast, when the set of conditions $x = \Delta_p/\Gamma_3 = 1$, $y = \Delta_c/\Gamma_3 = 0$, and $z = |\Omega_c|/\Gamma_3 = 100$ are met, the reflectance and transmittance are difficult to distinguish at each corresponding temperature, with values of 0.02948 and 0.03206, respectively, leading to difficulties in resolving the operating temperature between 283 K and 323 K.

Table 1. Reflectance and transmittance data of EIT vapor for proper coating temperature.

Temp.		Condition		$x = 1,$ $y = 0,$ $z = 10.$		$x = 1,$ $y = 0,$ $z = 50.$		$x = 1,$ $y = 0,$ $z = 80.$		$x = 1,$ $y = 0,$ $z = 100.$	
		T (K)	T (°C)	Refl.	Trans. ($\times 10^{-9}$)	Refl.	Trans. ($\times 10^{-7}$)	Refl.	Trans.	Refl.	Trans.
	283	10	0.999482	6.266	0.996913	7.735	0.002866	0.922671	0.017826	0.964154	
	288	15	0.999474	6.372	0.996955	7.237	0.023542	0.897178	0.020719	0.960617	
	293	20	0.999466	6.481	0.996995	6.794	0.067918	0.849543	0.02835	0.957449	
	298	25	0.999459	6.592	0.997033	6.397	0.134662	0.781554	0.027216	0.953753	
	303	30	0.999451	6.706	0.997069	6.041	0.218222	0.698869	0.020811	0.949835	
	308	35	0.999443	6.823	0.997103	5.720	0.310514	0.609308	0.034628	0.945704	
	313	40	0.999435	6.943	0.997135	5.431	0.403412	0.520487	0.038658	0.941369	
	318	45	0.999427	7.066	0.997165	5.169	0.490679	0.438072	0.042889	0.936839	
	323	50	0.999419	7.192	0.997194	4.931	0.568649	0.365234	0.047311	0.932129	
Range			0.000063	0.9266	0.000282	2.803	0.565782	0.557437	0.029485	0.032026	

Coatings on biological microelectromechanical systems (bioMEMSs) have a broad range of applications [34], with biomimetic micro- and nanotechnology experiencing substantial growth in recent years, leading to substantial advancements in the pharmaceutical

and biomedical fields. This has resulted in the development of new and improved devices, materials, tools, and operating-temperature-measuring (controlling) issues in various applications. In addition to temperature detection, the present mechanism can be used to measure electric and magnetic field strengths in some microelectromechanical systems. Static electric and magnetic fields can cause an energy eigenvalue shift in atomic energy levels (the Stark and Zeemann effects), which leads to changes in frequency detuning in the atomic polarizability and dielectric permittivity of an atomic vapor. Therefore, if a micron-scale atomic vapor cell can be embedded into a microelectromechanical system, the optical response of the vapor cell to an external control field and a probe light can be used to detect the electric and magnetic fields within the microelectromechanical system.

Figure 4 presents a schematic representation of the proposed experimental setup for a temperature-sensing device. This device is constructed with an electromagnetically induced transparency vapor slab, with a thickness of $1.2 \lambda_p$ (wavelength of probe field), positioned between two glass walls, each with a thickness of $0.5 \lambda_p$.

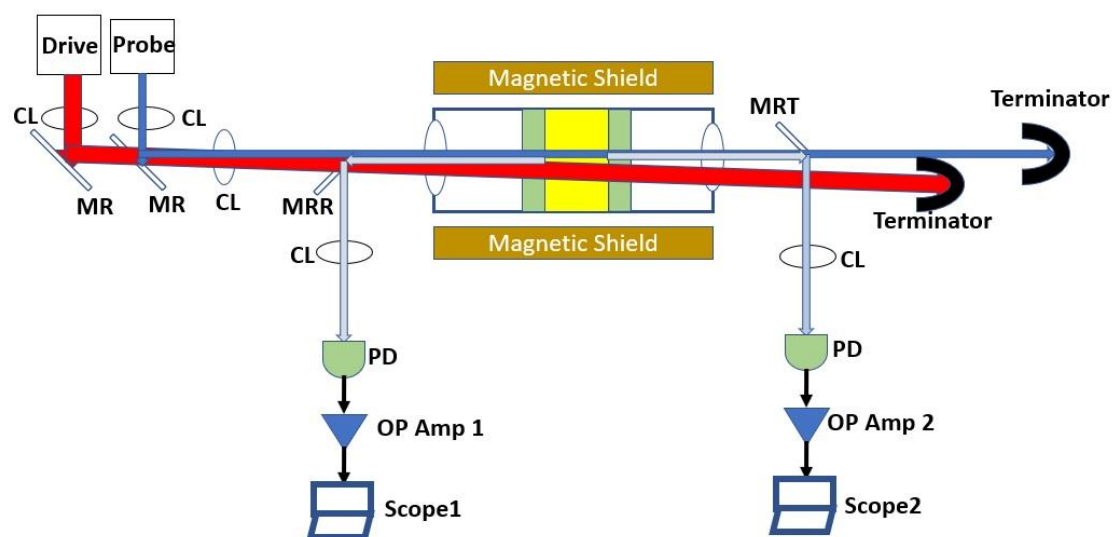


Figure 4. A scheme of temperature-sensing system via EIT vapor. In this setup, the strong driving (coupling) field is drawn as a wide red color beam, and the weak probe field is drawn as a normal blue color beam. CL represents a convex lens, BS denotes a beam splitter, PD is a kind of sensitive photodiode, and MR denotes a perfect reflecting mirror. MRR denotes a perfect mirror for reflected light, and MRT denotes a perfect mirror for transmitted light. OP Amps 1 and 2 are two accurate instrumental differential operational amplifiers, which can detect a very small electrical voltage (micro-voltage level).

5. Conclusions

The integration of special coating technologies with electromagnetically induced transparency (EIT) ensembles, embedded as randomly distributed inclusions or bubbles within a coating layer (e.g., GaAs and InGaAs), offers a wide-range visible probe light, with the potential for unprecedented levels of precision and control in temperature-sensing and coating processes. When the driving field strength is exactly 80 times that of the SDR, the EIT vapor system achieves reflectance and transmittance values ranging from 0 to 1, providing a direct indication of the corresponding temperature between 0 K and 600 K. To meet specific temperature range requirements, an EIT vapor slab temperature-sensing system could be designed by adjusting the adaptive intensity of the driving (coupling) field. In other words, we could unlock new possibilities for flexible-temperature-range-sensing systems by adaptively controlling the driving field in the EIT vapor.

Notably, this paper only describes a theoretical study based on atomic gas medium optics, where all the physical parameters need to be determined specifically through a physical model that includes atomic-level transition dynamics, the gaseous atom Doppler

effect, atomic gas optical properties, alkali-metal solid sublimation, and a saturated vapor density analysis. The method presented in this paper is suggested from a purely theoretical perspective. Because the temperature range of atomic vapor is wide (i.e., several hundred degrees kelvin), the dependence of the latent heat (related to alkali-metal solid sublimation) and saturated vapor density on the temperature cannot be expressed using simple functions, i.e., they need to be determined through experiments. Practical temperature-sensing mechanisms need to be determined using semi-empirical and semi-theoretical methods. In turn, the ideas, theory, and method presented in this paper may also be employed for determining the temperature-dependent behavior of the phase-transition latent heat and saturated vapor densities of alkali-metal elements.

In future applications, a temperature detector could be used to monitor changes in the EIT vapor slab. This would provide valuable information about the system's behavior and could lead to further advancements in our understanding of EIT optical phenomena in practical environments. Overall, the study of the effect of temperature on reflectance and transmittance in multilevel atomic vapor slabs is an area that deserves further attention because of its potential applications in photonic device design.

Author Contributions: The fundamental theoretical mechanism for temperature sensing with three-level atomic systems and vapor was suggested by J.-Q.S. Further conceptualization, methodology, software, validation, and writing of the original draft were completed by T.-C.L. Formal analysis, investigation, resources, data curation, writing (review and editing), visualization, and supervision were performed by J.-Q.S. and S.-F.S. All authors have read and agreed to the published version of the manuscript.

Funding: This study was supported in part by the National Natural Science Foundations of China, under grant no. 62105282, and the Ningbo Science and Technology Project, under grant no. 2021Z030. This work was also supported in part by the National Science and Technology Council (NSTC) of Taiwan, under grant no. NTSC-112-2221-E-011-140.

Institutional Review Board Statement: Not applicable.

Informed Consent Statement: Not applicable.

Data Availability Statement: Not applicable.

Conflicts of Interest: The authors declare no conflict of interest.

Appendix A

Three levels of some typical neutral atoms [27–30].

Doppler-Shift Ratio (Unit: s/m)	Lithium [27]	Sodium [28]	Lead [29]	Strontium [30]	Atom in This Study $m = 10$ AMU
k_{31}	1.1457	0.9508	1.1085	0.9317	1.1
k_{21}	0.8547	0.8087	0.3345	0.381	1.1×10^{-6}
k_{32}	0.291	0.1421	0.774	0.5507	1.1

References

1. Root, W.; Bechtold, T.; Pham, T. Textile-Integrated Thermocouples for Temperature Measurement. *Materials* **2020**, *13*, 626–648. [CrossRef]
2. Pourteimoor, S.; Haratizadeh, H. Performance of a Fabricated Nanocomposite-Based Capacitive Gas Sensor at Room Temperature. *J. Mater. Sci. Mater. Electron.* **2017**, *28*, 18529–18534. [CrossRef]
3. Blasdel, N.J.; Wujcik, E.K.; Carletta, J.; Lee, K.S.; Monty, C.N. Fabric Nanocomposite Resistance Temperature Detector. *IEEE Sens. J.* **2015**, *15*, 300–306. [CrossRef]
4. Katerinopoulou, D.; Zalar, P.; Sweetssen, J.; Kiriakidis, G.; Rentrop, C.; Groen, P.; Gerwin, H.; Gelinck, G.H.; Van der Brand, J.; Smit, E. Large-Area All-Printed Temperature Sensing Surfaces Using Novel Composite Thermistor Materials. *Adv. Electron. Mater.* **2018**, *5*, 605–611. [CrossRef]
5. Eriksson, P.; Andersson, J.Y.; Stemme, G. Thermal Characterization of Surface-Micromachined Silicon Nitride Membranes for Thermal Infrared Detectors. *J. Microelectromechanical Syst.* **1997**, *6*, 55–61. [CrossRef]

6. Cheng, L.; Steckl, A.J.; Scofield, J.D. Effect of Trimethylsilane Flow Rate on the Growth of SiC Thin-Films for Fiber-Optic Temperature Sensors. *J. Microelectromechanical Syst.* **2003**, *12*, 797–803. [[CrossRef](#)]
7. Scully, M.O.; Zubairy, M.S. *Quantum Optics*; Cambridge University Press: Cambridge, UK, 1997; pp. 220–245. ISBN 978-0-521-43595-6.
8. Cohen, J.L.; Berman, P.R. Amplification Without Inversion: Understanding Probability Amplitudes, Quantum Interference, and Feynman Rules in a Strongly Driven System. *Phys. Rev. A* **1997**, *55*, 3900–3917. [[CrossRef](#)]
9. Zhu, S.Y.; Scully, M.O. Spectral Line Elimination and Spontaneous Emission Cancellation via Quantum Interference. *Phys. Rev. Lett.* **1996**, *76*, 388–391. [[CrossRef](#)]
10. Krowne, C.M.; Shen, J.Q. Dressed-State Mixed-Parity Transitions for Realizing Negative Refractive Index. *Phys. Rev. A* **2009**, *79*, 023818. [[CrossRef](#)]
11. Shen, J.Q. Negatively Refracting Atomic Vapour. *J. Mod. Opt.* **2007**, *53*, 2195–2205. [[CrossRef](#)]
12. Shen, J.Q.; Zhang, P. Double-Control Quantum Interferences in a Four-Level Atomic System. *Opt. Express* **2007**, *15*, 6484–6493. [[CrossRef](#)]
13. Ye, C.Y.; Zibrov, A.S. Width of the Electromagnetically Induced Transparency Resonance in Atomic Vapor. *Phys. Rev. A* **2002**, *65*, 023806. [[CrossRef](#)]
14. Hockel, D.; Benson, O. Electromagnetically Induced Transparency in Cesium Vapor with Probe Pulses on the Single-Photon Level. *Phys. Rev. Lett.* **2010**, *105*, 153605. [[CrossRef](#)]
15. Finkelstein, R.; Bali, S.; Firstenberg, O.; Novikova, I. A Practical Guide to Electromagnetically Induced Transparency in Atomic Vapor. *New J. Phys.* **2023**, *53*, 035001. [[CrossRef](#)]
16. Lu, B.L.; Burkett, W.H.; Xiao, M. Electromagnetically Induced Transparency with Variable Coupling-Laser Linewidth. *Phys. Rev. A* **1997**, *56*, 976–979. [[CrossRef](#)]
17. Zhu, Y.; Wasserlauf, T.N. Sub-Doppler Linewidth with Electromagnetically Induced Transparency in Rubidium Atoms. *Phys. Rev. A* **1996**, *54*, 3653–3656. [[CrossRef](#)]
18. Taichenachev, A.V.; Tumaikin, A.M.; Yudin, V.I. Influence of Atomic Motion on the Shape of Two-Photon Resonance in Gas. *JETP Lett.* **2000**, *72*, 119–122. [[CrossRef](#)]
19. Karawajczyk, A.; Zakrzewski, J. Lasers Without Inversion in a Doppler-Broadened Medium. *Phys. Rev. A* **1995**, *51*, 830–834. [[CrossRef](#)]
20. Wang, D.Z.; Gao, J.Y. Effect of Doppler Broadening on Optical Gain Without Inversion in a Four-Level Model. *Phys. Rev. A* **1995**, *52*, 3201–3208. [[CrossRef](#)]
21. Lee, H.; Rostovtsev, Y.; Bednar, C.J.; Javan, A. From Laser-Induced Line Narrowing to Electromagnetically Induced Transparency: Closed System Analysis. *Appl. Phys. B* **2003**, *76*, 33–39. [[CrossRef](#)]
22. Born, M.; Wolf, E. *Principles of Optics*, 7th ed.; Cambridge University Press: Cambridge, UK, 1999; pp. 401–424. ISBN 0-08-026482-4.
23. Liu, N.H.; Zhu, S.Y.; Chen, H.; Wu, X. Superluminal Pulse Propagation through One-dimensional Photonic Crystals with a Dispersive Defect. *Phys. Rev. E* **2002**, *65*, 046607. [[CrossRef](#)]
24. Shen, J.Q.; Zeng, R.X. Quantum-Coherence-Assisted Tunable On- and Off-Resonance Tunneling through a Quantum-Dot-Molecule Dielectric Film. *J. Phys. Soc. Jpn.* **2017**, *86*, 024401. [[CrossRef](#)]
25. Jafari, D.; Sahrai, M.; Motavali, H.; Mahmoudi, M. Phase Control of Group Velocity in a Dielectric Slab Doped with Three-Level Ladder-Type Atoms. *Phys. Rev. A* **2011**, *84*, 068311. [[CrossRef](#)]
26. Zeng, R.; Gu, J.; Shen, J.Q. Controllable Tunneling of Light through a Quantum-Dot-Molecule Dielectric Film via Electromagnetically Induced Transparency. *Opt. Photonics J.* **2017**, *7*, 49–67. [[CrossRef](#)]
27. Radziemski, L.J.; Engleman, R.J.; Brault, J.W. Fourier-Transform-Spectroscopy Measurements in the Spectra of Neutral Lithium, ^6I and ^7I (Li I). *Phys. Rev. A* **1995**, *52*, 4462–4470. [[CrossRef](#)]
28. Martin, W.C.; Zalubas, R. Energy Levels of Sodium, NO I through Na XI. *J. Phys. Chem. Ref. Data* **1981**, *10*, 153–194. [[CrossRef](#)]
29. Kasapi, A. Enhanced Isotope Discrimination Using Electromagnetically Induced Transparency. *Phys. Rev. Lett.* **1996**, *77*, 1035–1038. [[CrossRef](#)]
30. Boiler, K.J.; Imamoglu, A.; Harris, S.E. Observation of Electromagnetically Induced Transparency. *Phys. Rev. Lett.* **1991**, *66*, 2593–2596. [[CrossRef](#)]
31. Wang, Z.C. *Thermodynamics and Statistical Physics*, 3rd ed.; Higher Education Press: Beijing, China, 2003; ISBN 978-7040226362.
32. Talebian, E.; Talebian, M. A General Review on the Derivation of Clausius–Mossotti Relation SciVerse ScienceDirect. *Optik* **2013**, *124*, 2324–2326. [[CrossRef](#)]
33. *ASTM D3276-86*; Standard Guide for Painting Inspectors (Metal Substrates). ASTM International: West Conshohocken, PA, USA, 2021; p. 174.
34. Abbas, A.; Huang, S.J. Investigating the Synergic Effects of WS₂ and ECAP on Degradation Behavior of AZ91 Magnesium Alloy. *Coatings* **2022**, *12*, 1710–1721. [[CrossRef](#)]

Disclaimer/Publisher’s Note: The statements, opinions and data contained in all publications are solely those of the individual author(s) and contributor(s) and not of MDPI and/or the editor(s). MDPI and/or the editor(s) disclaim responsibility for any injury to people or property resulting from any ideas, methods, instructions or products referred to in the content.